Dalton Transactions

ROYAL SOCIETY OF CHEMISTRY

PAPER

View Article Online
View Journal | View Issue

Cite this: *Dalton Trans.*, 2021, **50**, 6949

Synthesis, characterization and thermal behaviour of solid phases in the quasi-ternary system $Mg(SCN)_2$–H_2O–THF†

Markus Joos,[a] Maurice Conrad,[b] Rotraut Merkle,[a] Thomas Schleid,[b] Joachim Maier,[a] Robert E. Dinnebier[a] and Sebastian Bette*[a,b]

$Mg(SCN)_2{\cdot}4H_2O$ can be converted into previously unknown compounds $Mg(SCN)_2{\cdot}(4-x)\ H_2O{\cdot}x$THF with x = 0, 2 and 4 by multiple recrystallization in tetrahydrofuran (THF). The phases were characterized by infrared spectroscopy (IR), thermogravimetric analysis (TGA) and differential scanning calorimetry (DSC), and their crystal structures were solved from X-ray powder diffraction (XRPD) data. In the crystal structures isolated $Mg(NCS)_2(H_2O)_{4-x}(THF)_x$ units form layered motifs. The thermal behavior of $Mg(SCN)_2{\cdot}4H_2O$ and $Mg(SCN)_2{\cdot}4$THF was investigated by temperature dependent *in situ* XRPD, where $Mg(SCN)_2{\cdot}4$THF was found to acquire a room temperature (α-form) and high temperature modification (β-form). The phase transformation is associated with an order–disorder transition of the THF molecules and with a reversion of the stacking order of the layered motifs. Further heating eventually leads to the formation of $Mg(SCN)_2{\cdot}2$THF. There thiocyanate related sulfur atoms fill the voids in the coordination sphere of magnesium, which leads to the formation of one dimensional electroneutral $_\infty[Mg(NCS)_{2/2}(SCN)_{2/2}(THF)_2]$ chains. All investigated $Mg(SCN)_2{\cdot}(4-x)\ H_2O{\cdot}x$THF phases exhibit a remarkable anisotropic thermal expansion, and $Mg(SCN)_2{\cdot}4H_2O$ and $Mg(SCN)_2{\cdot}2$THF were found to show both positive and negative thermal expansion coefficients.

Received 11th February 2021,
Accepted 15th April 2021

DOI: 10.1039/d1dt00469g

rsc.li/dalton

Introduction

Magnesium halides and pseudo-halides exhibit a great variety of chemical and structural properties and are used in many different applications, which is why they have been extensively studied.[1–5] However, in the row of magnesium pseudo-halides, *i.e.* cyanides, cyanates, azides *etc.*, thiocyanates are often overseen, and only little chemical and structural knowledge is available for magnesium thiocyanates and their derivatives.

The first known crystalline magnesium thiocyanate phase was reported to be the tetrahydrate $Mg(SCN)_2{\cdot}4H_2O$ in 1930,[6] which was later confirmed by the elucidation of its crystal structure.[7] In addition, some reports have mentioned the existence of related phases, such as the pentahydrate $Mg(SCN)_2{\cdot}5H_2O$ or anhydrous $Mg(SCN)_2$;[8–11] however, only little to no evidence was presented to support this. Several studies showed that Mg^{2+} when coordinated to SCN^- anions seems to be capable to form a diversity of solid ionic complexes with different organic molecules such as pyridine (Py), nicotinamide (NIA) and their derivatives,[10–13] although their crystal structures remain unknown.

Besides the tetrahydrate $Mg(SCN)_2{\cdot}4H_2O$, crystal structure investigations of $Mg(SCN)_2$-containing compounds have generally been neglected so far and only spectroscopic studies or thermal analyses are present.[10,12] Further structural studies of related Mg^{2+}-SCN^--phases are only available for mixed cationic systems involving other cations like K^+ or Cd^{2+}.[14,15] In contrast, other MgX_2 salts with similar anions (X = CN, $N(CN)_2$) are well known in terms of crystal structures and properties.[16,17]

Furthermore, unlike many other thiocyanate salts $M(SCN)_n$ (M = Li, Na, K, Ca, Sr, Ba, Ni, Ag, Hg, ..., n = 1 or 2),[18–25] it is yet unclear how to obtain the anhydrous form of $Mg(SCN)_2$ and under what conditions it would be stable. As mentioned before, some studies suggest the formation of anhydrous $Mg(SCN)_2$ by simple heating of $Mg(SCN)_2{\cdot}x$ [L] complexes ([L] = H_2O, pyridine, ...);[10] however, the phase formation was not

[a]*Max Planck Institute for Solid State Research, Heisenbergstr. 1, 70569 Stuttgart, Germany. E-mail: S.Bette@fkf.mpg.de*
[b]*Institut für Anorganische Chemie, University of Stuttgart, Pfaffenwaldring 55, 70569 Stuttgart, Germany*

†Electronic supplementary information (ESI) available. CCDC 2055308–2055312. For ESI and crystallographic data in CIF or other electronic format see DOI: 10.1039/d1dt00469g

analytically confirmed in any case. In fact, a more likely dehydration mechanism might be similar to that of $MgCl_2$, which forms a wide variety of hydrates.[1,2,26–28] The hexahydrate $MgCl_2{\cdot}6H_2O$ is a commonly occurring mineral named bischofite and finds a diversity of industrial usage.[1–4,29] Upon heating of $MgCl_2$ hydrates different dehydration stages occur; however, the anhydrous state cannot simply be reached as the formation of oxychloride species prevails.[2,3,27] Solvent based methods or rather tedious thermochemical procedures are necessary to produce pure, anhydrous $MgCl_2$.[3]

Besides the rich hydrate chemistry of $MgCl_2$, it also forms different organometallic complexes, which are of great importance in organic chemistry (such as Grignard reagents or for Ziegler–Natta catalysis)[30–33] and have more recently even sparked interest in the battery community.[34] These complexes are formed by the inclusion of organic molecules such as pyridine (Py), dimethoxyethane (DME), tetrahydrofuran (THF) *etc.*, and a lot of research studies are devoted to their structural analysis, especially to understand the coordination between metals and organic molecules.[30,33–38]

Moving on from halides to pseudo-halides, the previously mentioned coordination chemistry between metals and organic molecules is still a rather unexplored field for crystalline, solid thiocyanates. Some examples of solvent complexes with dimethoxyethane (DME), tetrahydrofuran (THF) and acetonitrile (AN) can be found for rare earth metal thiocyanates and $Ca(SCN)_2$.[39] There also exist coordination compounds with acetone (Ac) of transition metals (TM = Cr, Mn and Fe);[40] yet for $Mg(SCN)_2$, only little is known about these kinds of complexes and no structural data are available so far.

In this study we report the synthesis, structure, spectroscopic properties and thermal behavior of the solid phases dithiocyanatetetraaquamagnesium(II) $[Mg(SCN)_2(H_2O)_4]$ (also referred to as magnesium dithiocyanate tetrahydrate, $Mg(SCN)_2{\cdot}4H_2O$), bis(tetrahydrofuran)diaquadi-thiocyanatemagnesium(II), $[Mg(SCN)_2(H_2O)_2(THF)_2]$, and dithiocyanatetetrakis(tetrahydrofuran)-magnesium(II), $[Mg(SCN)_2(THF)_4]$ (from hereon we will address these compounds as $Mg(SCN)_2{\cdot}(4-x)\,H_2O{\cdot}x$THF with x = 0, 2, 4).[41] The thermal behaviour of the title compounds was analysed in detail by temperature dependent *in situ* X-ray powder diffraction and a strong anisotropic lattice expansion as well as several phase transitions of $Mg(SCN)_2{\cdot}4$THF eventually leading to the formation of $Mg(SCN)_2{\cdot}2$THF were observed.

Experimental

$Mg(SCN)_2{\cdot}(4-x)\,H_2O{\cdot}x$THF ($x$ = 0, 2, 4) phases were synthesized by recrystallization in H_2O or THF or by ion exchange. The obtained products were characterized by X-ray powder diffraction (XRPD), infrared (IR) spectroscopy, thermogravimetric analysis (TGA), differential scanning calorimetry (DSC), scanning electron microscopy (SEM) and energy dispersive X-ray (EDX) analysis. The handling and measurements of the samples were conducted under dry inert gas or vacuum unless stated otherwise. All details of the synthesis and analysis can be found in the ESI.†

Results

Synthesis and characterization

Syntheses of $Mg(SCN)_2{\cdot}4H_2O$ have been reported in a number of different publications employing various synthesis routes, such as:[6–8,10–12]

$$\begin{aligned} &Mg(OH)_2 + 2HSCN(+2NH_4SCN) + 2H_2O \rightarrow \\ &Mg(SCN)_2 \cdot 4H_2O\ (+2NH_3\uparrow) \\ &MgCO_3 + 2HSCN\ (+2NH_4SCN) + 3H_2O \rightarrow \\ &Mg(SCN)_2 \cdot 4H_2O + CO_2\uparrow (+2NH_3\uparrow) \end{aligned} \quad (1)$$

$$\begin{aligned} &MgSO_4 \cdot 7H_2O + Ba(SCN)_2 \cdot 3H_2O \rightarrow \\ &Mg(SCN)_2 \cdot 4H_2O + BaSO_4\downarrow + 6H_2O \end{aligned} \quad (2)$$

$$\begin{aligned} &MgCl_2 \cdot 6H_2O + KSCN \xrightarrow{EtOH} \\ &Mg(SCN)_2 \cdot 4H_2O + KCl\downarrow + 2H_2O \end{aligned} \quad (3)$$

The third synthesis route is employed in this study. However, it was discovered that after the removal of ethanol, the formation of $Mg(SCN)_2{\cdot}4H_2O$ crystals was severely inhibited, and precipitation required long vacuum treatment at rather high temperatures (~150 °C) with the possible formation of decomposition products. A much easier way to produce crystalline $Mg(SCN)_2{\cdot}4H_2O$ without risking decomposition was, after removing most of the ethanol, to re-dissolve the obtained slurry in water and then use freeze drying to precipitate the crystals of $Mg(SCN)_2{\cdot}4H_2O$. Nonetheless, the purity of $Mg(SCN)_2{\cdot}4H_2O$ for both the synthesis routes 2 and 3 is limited due to the solubility product of $BaSO_4$ in water (1.3×10^{-5} mol L^{-1})[42] and KCl in ethanol (3.9×10^{-5} mol L^{-1}).[43] This problem does not occur in the synthesis route 1; however, additional heat treatments or neutralization is required to entirely remove NH_3 or CO_2. To avoid the limits created by these methods, we used cation exchange *via* an ion exchanger, which directly yielded pure $Mg(SCN)_2{\cdot}4H_2O$ without further treatments being necessary. Low requirements on the metal-base purity of the precursor KSCN are an additional advantage of this method, as impurity cations contained within the commercially available precursor material will be replaced by Mg^{2+} cations as well.

Both the syntheses of $Mg(SCN)_2{\cdot}2H_2O{\cdot}2$THF and $Mg(SCN)_2{\cdot}4$THF required an additional re-crystallization step using THF as the solvent. It was difficult to control the ratio of H_2O to THF, especially for $Mg(SCN)_2{\cdot}2H_2O{\cdot}2$THF, and several synthesis attempts produced a mixture of both $Mg(SCN)_2{\cdot}2H_2O{\cdot}2$THF and $Mg(SCN)_2{\cdot}4$THF (Fig. 1). In the case of $Mg(SCN)_2{\cdot}4$THF, this problem could be overcome by simply refluxing the solution in THF to remove any remaining H_2O, although this might have caused the formation of an amorphous side phase (more details can be found in the ESI†). With the above described methods three phases with x = 0, 2, 4 in the ternary system $Mg(SCN)_2{\cdot}(4-x)\,H_2O{\cdot}x$THF were suc-

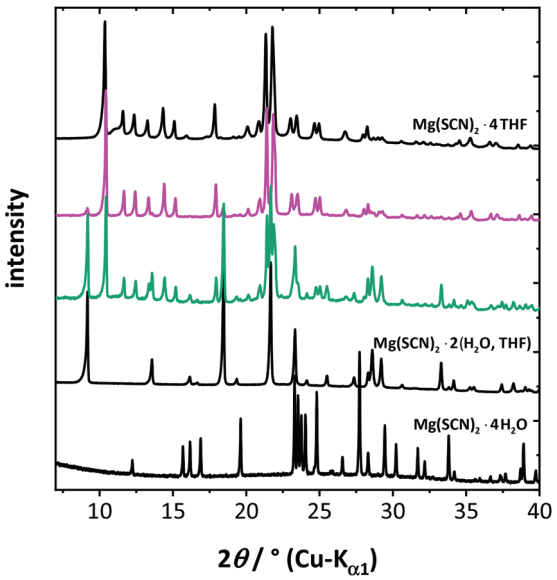

Fig. 1 XRPD patterns of the series $Mg(SCN)_2{\cdot}(4-x)\ H_2O{\cdot}x$THF showing different syntheses products; pure phases (black) and mixed phases (colored).

Table 1 Crystallographic data for all $Mg(SCN)_2{\cdot}(4-x)\ H_2O{\cdot}x$THF phases

	$x = 0$	$x = 2$	$x = 4$
Space group	$P2_1/a$	$C2/m$	$P2_1/n$
a/Å	7.4947(1)	10.7474(2)	15.2137(8)
b/Å	9.0296(1)	8.1893(1)	10.2054(4)
c/Å	7.8721(1)	9.6299(2)	7.7220(3)
β/°	113.650(1)	93.153(1)	94.980(2)
V/Å	488.00(1)	846.29(3)	1194.39(9)
Z	2	2	2

cessfully synthesized, all of which crystallize in a monoclinic lattice (Table 1).

The exchange of water with THF molecules leads to fundamental changes in the crystal lattice. From $x = 0$ to $x = 2$, the volume per formula unit strongly increases by 179.15 Å^3, illustrated by the strong downshift of the 001 reflection. This increase is smaller than the volume of two free THF molecules (269 Å^3). The SEM images in Fig. S4a and b† show that the grain morphologies become more platelet like, which indicated a more pronounced layered motif in the crystal structure after the THF incorporation. When the THF content is increased from $x = 2$ to $x = 4$, the volume per formula unit increases by 174.05 Å^3, which is very similar to the first exchange step. The C-centered monoclinic unit cell becomes primitive (space group $P2_1/n$ for $x = 4$) upon complete exchange.

Furthermore, the grains adopt a rod-shaped morphology with well-defined crystal faces, as can be seen in Fig. S4c.† The EDX results of $x = 4$ shown in Fig. S5† match the proposed stoichiometry with an average Mg : S ratio of 1 : 2.

IR spectroscopy was employed to confirm the presence of thiocyanate and THF as well as to derive information on the coordination of Mg^{2+}. Fig. 2 shows selected excerpts of the IR spectra for all $Mg(SCN)_2{\cdot}(4-x)\ H_2O{\cdot}x$THF phases.

The spectra show THF and water related bands situated in the high wavenumber region between 2800 and 3600 cm^{-1}. For $Mg(SCN)_2{\cdot}4H_2O$ and $Mg(SCN)_2{\cdot}4$THF the bands of THF and H_2O are respectively absent (Fig. 2, black and orange line), while the spectrum of $Mg(SCN)_2{\cdot}2H_2O{\cdot}2$THF shows a combination of both (Fig. 2, blue line; further details can be found in Table 2). Interestingly, the characteristic bands ν(C≡N) (~2080 cm^{-1}) and δ(H–O–H) (~1630 cm^{-1}) of the SCN^- anion and H_2O are split for $Mg(SCN)_2{\cdot}4$THF and $Mg(SCN)_2{\cdot}2H_2O{\cdot}2$THF, respectively. In the case of the SCN^- anion, such a splitting was also observed for the dihydrate $Ca(SCN)_2{\cdot}2H_2O$,[21] the trihydrate $K_2Mg_2(SCN)_6{\cdot}3H_2O$,[14] and various rare earth metal thiocyanate complexes with different solvent molecules.[39] In the last case, the splitting was attributed to the bridging nature of SCN^- to two cations, enabling both symmetric and asymmetric ν(C≡N) modes. In contrastry, here SCN^- does not have a bridging function (see below), and

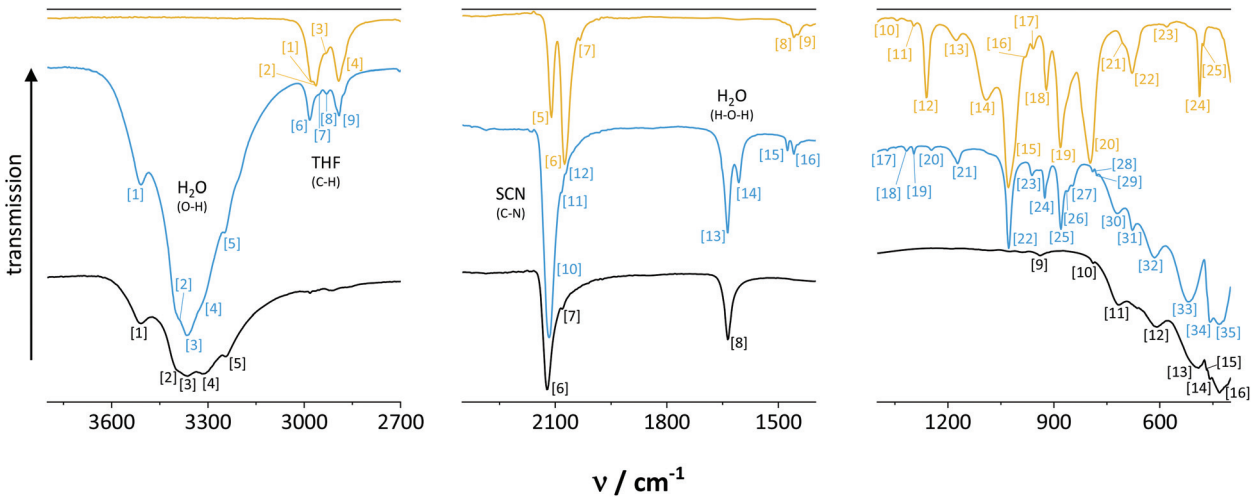

Fig. 2 IR spectra of $Mg(SCN)_2{\cdot}(4-x)\ H_2O{\cdot}x$THF phases with $x = 0$ (black, measured in Ar), $x = 2$ (blue, measured in air), $x = 4$ (orange, measured in Ar).

Table 2 Wavenumbers of IR spectra in Fig. 2 for all $Mg(SCN)_2 \cdot (4-x)H_2O \cdot xTHF$ phases with tye respective assignments according to the literature[18,21,44–46]

$x = 0$; ν/cm^{-1}	$x = 2$; ν/cm^{-1}	$x = 4$; ν/cm^{-1}	Assignment
[1] 3511	[1] 3509		ν_2(O–H) [H_2O]
[2] 3400	[2] 3402		
[3] 3363	[3] 3365		
[4] 3314	[4] 3328		
[5] 3244	[5] 3247		ν_1(O–H) [H_2O]
	[6] 2982	[1] 2977	ν_2(C–H) [THF]
	[7] 2955	[2] 2963	
	[8] 2931	[3] 2932	
	[9] 2892	[4] 2893	ν_1(C–H) [THF]
[6] 2123	[10] 2117	[5] 2110	ν(C≡N) [SCN]
[7] 2081	[11] 2083		
	[12] 2072	[6] 2075	
		[7] 2034	
[8] 1636	[13] 1637		δ(H–O–H) [H_2O]
	[14] 1606		
	[15] 1476	[8] 1459	δ(H–C–H) [THF]
	[16] 1458	[9] 1447	
	[17] 1372		ω(H–C–H) [THF]
		[10] 1344	
	[18] 1318		
	[19] 1296	[11] 1296	
	[20] 1247	[12] 1261	
	[21] 1172	[13] 1177	ν_2(ring) [THF]
		[14] 1092	T(H–C–H) [THF]
	[22] 1028	[15] 1028	ν_2(ring) [THF]
		[16] 981	2δ(S–C≡N) [SCN]
	[23] 962	[17] 958	ρ(H–C–H) [THF]
[9] 940			2δ(S–C≡N) [SCN]
	[24] 926	[18] 921	ν_1(ring) [THF]
	[25] 880	[19] 882	[THF]
	[26] 861		
	[27] 847		
[10] 789	[28] 790	[20] 797	ν(S–C) [SCN]
	[29] 778		
[11] 719	[30] 722		T(H–O–H) [H_2O]
		[21] 705	
	[31] 678	[22] 678	ρ(H–C–H) [THF]
[12] 610	[32] 616	[23] 581	δ(ring i–p) [THF]
[13] 495	[33] 518		
[14] 468		[24] 488	δ(S–C≡N) [SCN]
[15] 458	[34] 458	[25] 477	
[16] 432	[35] 432		

ν_1: symmetric stretch, ν_2: asymmetric stretch; δ: scissoring or bending; ω: wagging; T: twisting; ρ: rocking; i–p: in-plane.

it is more likely that the splitting is connected to the complexity of molecules coordinated to the central cation in the vicinity of SCN^-. Since this splitting does not appear in the bands of $Mg(SCN)_2 \cdot 4H_2O$, it can be attributed to the coordination of THF molecules to Mg^{2+}, inducing polarization effects either in H_2O or SCN^-. However, an unambiguous explanation requires a more rigorous treatment of the spectroscopic features of these phases and is beyond the scope of this report.

In summary, the combination of XRPD and IR spectroscopy shows that THF molecules can successfully be introduced into the structure of $Mg(SCN)_2$ producing new crystalline phases with distinct properties.

Thermal behavior

In the family of magnesium salts, $MgCl_2$ is a close relative to magnesium thiocyanate for which the thermal behaviour has already been studied thoroughly, especially regarding the complexity of obtaining pure, anhydrous $MgCl_2$.[2,3] In comparison, the hydrates of LiSCN, NaSCN and $Ca(SCN)_2$ were reported to be readily dehydrated by simple heating of the hydrated material.[18,19,21] Various anhydrous thiocyanate salts have been shown to melt congruently around 280–470 °C followed by decomposition above ~550 °C,[22] and bimetallic thiocyanates first dissociate before decomposing to sulphides and gaseous species.[15]

Fig. 3 shows the TGA measurement of $Mg(SCN)_2 \cdot 4H_2O$ along with the corresponding signals from mass spectroscopy (MS). According to the TGA and MS analyses, the tetrahydrate passes through different hydrates (nominal a dihydrate at 144 °C and nominal a monohydrate at 154 °C), until it finally decomposes starting around 161 °C. However, along with the recorded peaks for H_2O in the MS, another signal with a molar mass of 44 g mol^{-1} (*e.g.* CO_2) was observed, which could indicate that the dehydration is accompanied by a partial decomposition process already below 161 °C. The here recorded TGA measurement agrees with that from Mojumdar *et al.*,[10] even though the temperatures seem to be slightly shifted. Regarding the interpretation, however, some clarifications are necessary: (i) Given the hygroscopy of $Mg(SCN)_2 \cdot 4H_2O$, it is possible that the additional H_2O molecule reported in reference 10 was actually just adsorbed surface water. (ii) There is no evidence for the intermediate formation of anhydrous $Mg(SCN)_2$ and the MS analysis rather suggests a thermal decomposition. (iii) Even though the formation of MgS as a decomposition product is indeed possible and would be in line with other thiocyanate systems,[15] it remains challenging to substantiate this given the limited information obtainable by *e.g.* XRPD or IR spectroscopy (Fig. S9†).

Further TGA and DTA measurements of magnesium thiocyanate complexes with various incorporated organic molecules often show a step-wise mass loss of the organic molecule followed by thermal decomposition.[10,12] A similar mechanism was observed in the TGA measurement of $Mg(SCN)_2 \cdot 4THF$ (Fig. 4) concerning the loss of THF. According to the combi-

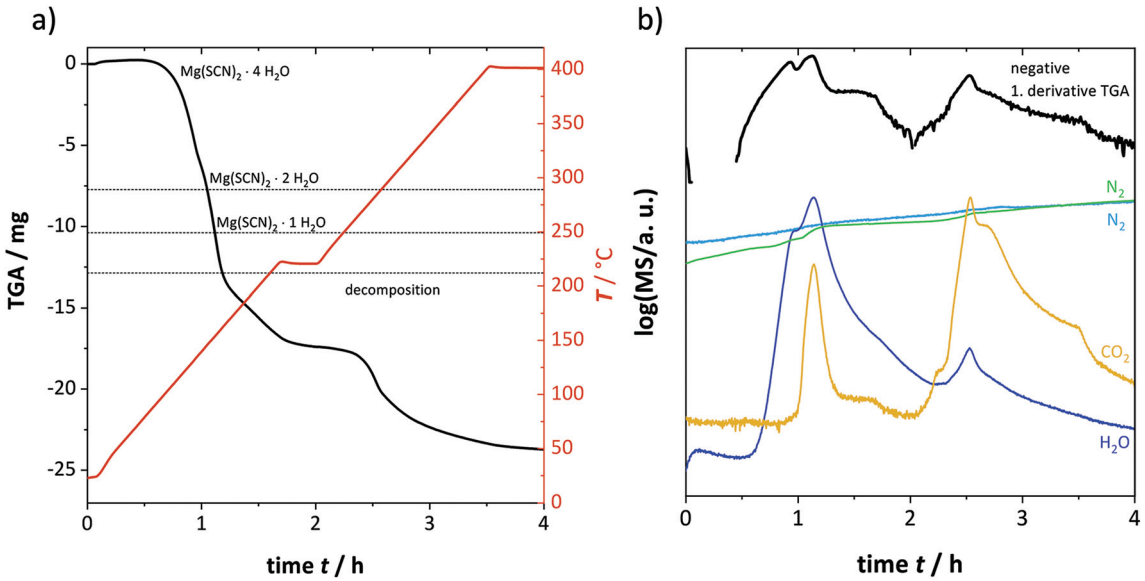

Fig. 3 TGA measurement of $Mg(SCN)_2{\cdot}4H_2O$ under N_2: (a) TGA signal; (b) MS signal.

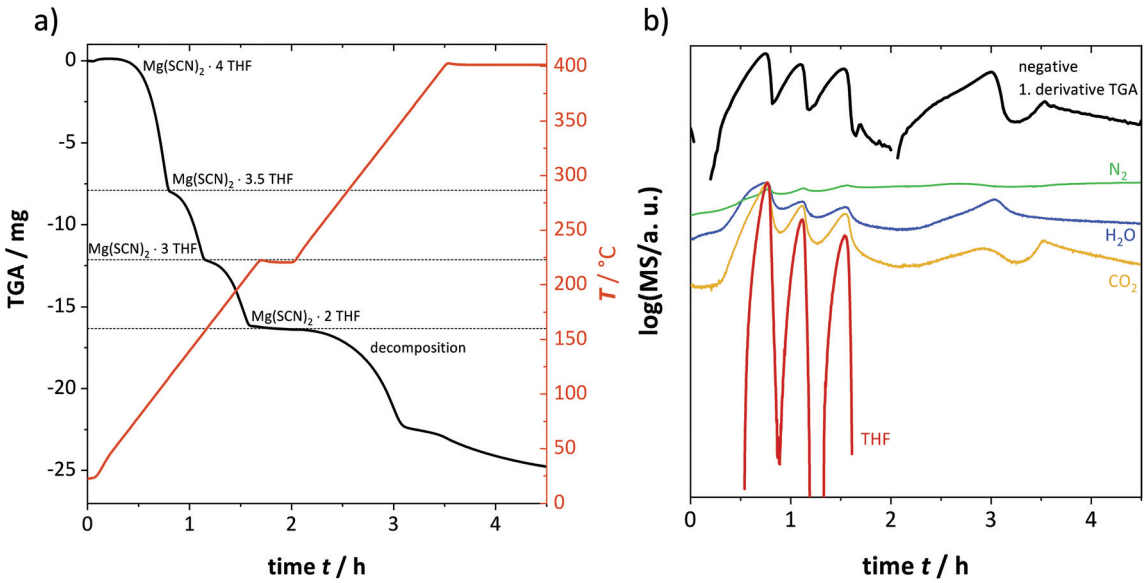

Fig. 4 TGA measurement of $Mg(SCN)_2{\cdot}4THF$ under N_2: (a) TGA signal; (b) MS signal.

nation of TGA and MS, three intermediates were formed with 3.5 (113 °C), 3 (156 °C) and 2THF (210 °C) molecules followed by thermal decomposition.

The thermal behavior of $Mg(SCN)_2{\cdot}4H_2O$ and $Mg(SCN)_2{\cdot}4THF$ was further investigated by DSC (Fig. 5). The DSC measurements showed that in a semi-closed system (cold welded aluminium pan) the tetrahydrate melts at 144 °C with a pronounced hysteresis (supercooling) effect as crystallization does not occur before 80 °C. Beyond 144 °C the material showed further endothermic peaks starting at 167 °C, indicating thermal decomposition. The decomposition temperature measured by DSC fits well to that observed by TGA in Fig. 3a. In contrast, $Mg(SCN)_2{\cdot}4THF$ displayed higher thermal stability than the tetrahydrate with the first endothermic peak occurring at 197 °C. This finding is rather counterintuitive, since the exchange of H_2O with organic ligands would be expected to decrease the thermal stability of the material. Thereafter two more endothermic peaks are observed at 219 °C and 279 °C. Since no exothermic peaks appear in the cooling run as well as considering the results from TGA, we can assume that the peak at 279 °C indicates the thermal decomposition of the material. Furthermore, the TGA measurement showed

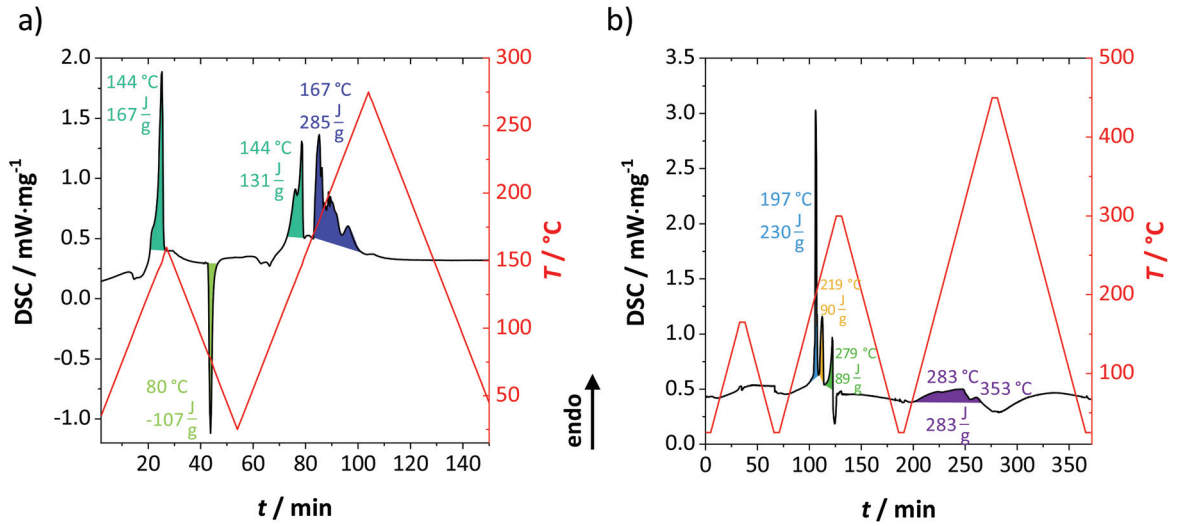

Fig. 5 DSC measurements of different phases in the series $Mg(SCN)_2 \cdot (4 - x)\ H_2O \cdot x THF$ shown for (a) $x = 0$ and (b) $x = 4$.

that at around 210 °C the material loses two THF molecules, which is connected with the DSC peaks at 197 °C and 219 °C. Subsequent heating to higher temperatures merely revealed further decomposition of the material.

In order to corroborate the above findings of TGA and DSC, temperature dependent *in situ* XRPD measurements were conducted for both $Mg(SCN)_2 \cdot 4H_2O$ and $Mg(SCN)_2 \cdot 4THF$ (Fig. 6). For the tetrahydrate, all reflections in the XRPD pattern disappear between 149 °C and 186 °C in agreement with the melting point at 144 °C and the decomposition at 167 °C from DSC. The formation of a new phase is observed at 190 °C, distinctly different from the originally present $Mg(SCN)_2 \cdot 4H_2O$ in terms of the XRPD pattern. Even though a structure solution of this emergent phase was not possible due to anisotropic peak broadening, it appears to be a yet unknown stacking faulted decomposition product of $Mg(SCN)_2 \cdot 4H_2O$.

$Mg(SCN)_2 \cdot 4THF$ undergoes several phase transitions upon heating before it melts or becomes amorphous (Fig. 6). At 138 °C a phase transition occurs from the parent structure α-$Mg(SCN)_2 \cdot 4THF$ to a new polymorphic phase β-$Mg(SCN)_2 \cdot 4THF$, evident from the changes in the XRPD pattern. It should be noted here that most likely this β-phase was not observed in the TGA measurement shown in Fig. 4, as THF first evaporated in the continuous N_2 gas stream of the TGA before the β-phase could form. Yet with the sealed capillary employed in the temperature dependent *in situ* XRPD measurement, THF is contained long enough in the sample for the β-phase to evolve. It remains unclear, however, why for the α- to β-transition no signal was observed in the DSC. Given the long measurement times in XRPD (hours for each temperature point), the kinetics of the phase transition are most likely slow. Furthermore, within the employed temperature ranges, any vibrational entropic contributions to the overall change in energy is probably small and difficult to resolve by DSC. It is therefore very likely that the phase transition could not be resolved by DSC and was consequently not observed. Upon further heating THF loss is inevitable until at 164 °C (DSC: 197 °C, TGA: 210 °C) a new phase starts to form yielding $Mg(SCN)_2 \cdot 2THF$. The formation temperature here is a bit lower than that observed by TGA and DSC, which can be attributed to both different measurement set-ups as well as a different environment from the gas phases (the closed system in XRPD, the semi-closed system in DSC and the open system in TGA). The new phase $Mg(SCN)_2 \cdot 2THF$ is stable up to 234 °C at which point, it first turns into an unknown, stacking faulted decomposition product and then finally melts or becomes amorphous starting around 251 °C (DSC: 279 °C).

The obvious differences in thermal behaviour between $Mg(SCN)_2 \cdot 4H_2O$ and $Mg(SCN)_2 \cdot 4THF$ are rather surprising, especially considering their similar coordination chemistry. Even though it appears counterintuitive for the tetrahydrate to have a lower thermal stability, as the formation of bridging hydrogen bonds should stabilize the structure, without having any knowledge of anhydrous $Mg(SCN)_2$, a direct comparison between the phases cannot be made analytically.

With both TGA and XRPD the formation of anhydrous $Mg(SCN)_2$ was not observed and it remains to be clarified under which conditions it could be obtained. The intermediately formed $Mg(SCN)_2 \cdot 2THF$ phase is to date the only magnesium thiocyanate with only two coordinating molecules. Regarding the progression of reflections in the XRPD patterns (Fig. 6b and d), a significant shifting of selected reflections to lower angles was observed for both phases. This shifting indicates a strong and possibly anisotropic lattice expansion, which we will address later in more detail. Given the delicate synthesis and storage of $Mg(SCN)_2 \cdot 2H_2O \cdot 2THF$, we decided to only report the results of room temperature measurements.

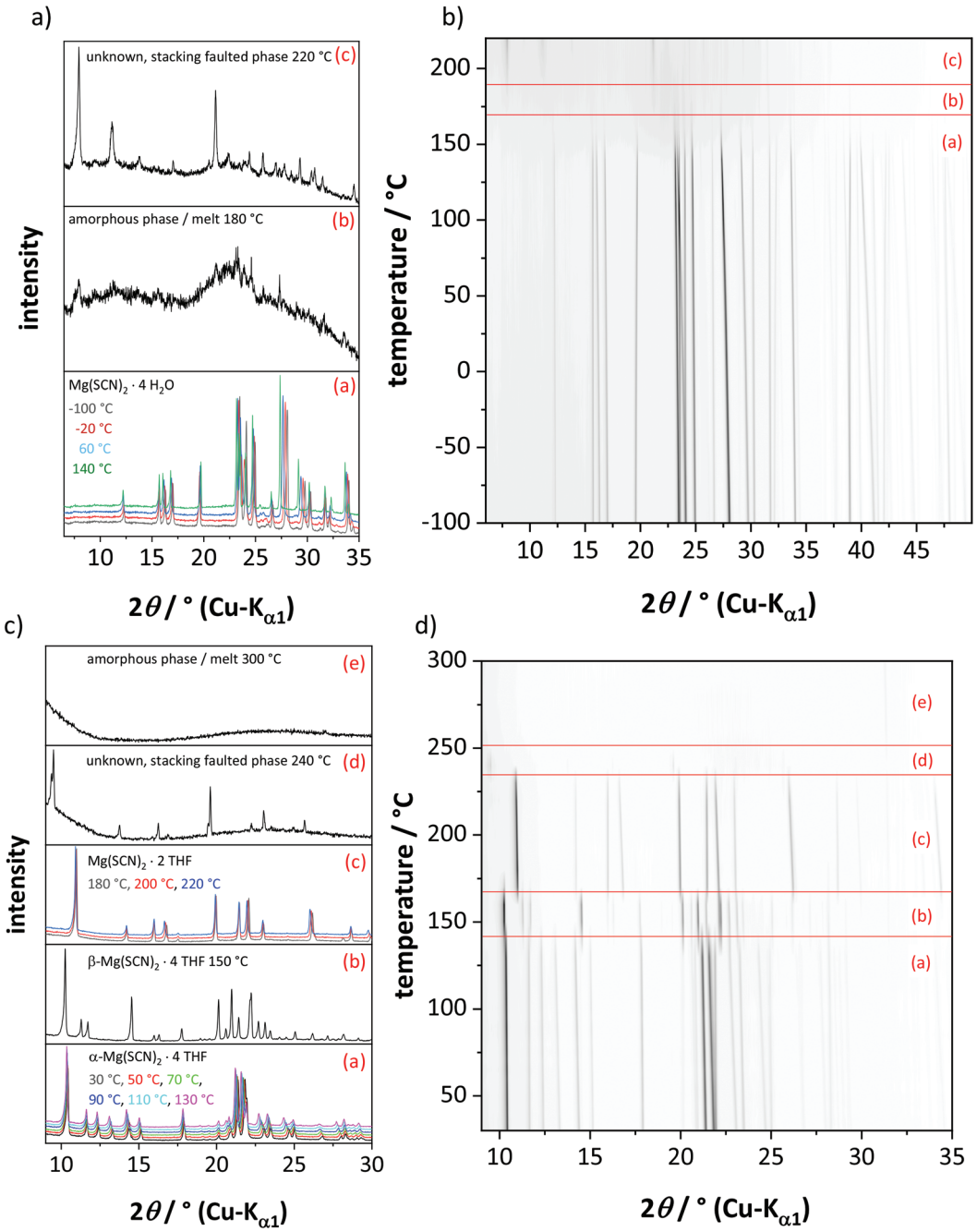

Fig. 6 Temperature dependent *in situ* XRPD data of $Mg(SCN)_2{\cdot}4H_2O$ (a and b) and $Mg(SCN)_2{\cdot}4THF$ (c and d) in a sealed capillary under Ar showing (a and c) selected XRPD patterns and (b and d) the thermal progression of reflections.

Structure description

In the series $Mg(SCN)_2{\cdot}(4-x)\ H_2O{\cdot}x$THF with $x = 0$, $x = 2$ and $x = 4$, the Mg^{2+} cations always exhibit a distorted octahedral coordination sphere with the thiocyanate anions located in the *trans* configuration with the N pointing towards Mg^{2+} (Fig. 7). In $Mg(SCN)_2{\cdot}4H_2O$ water molecules occupy the equatorial positions (Fig. 7a, green atoms) and the magnesium is situated on the centre of inversion. After replacing two water molecules by THF in $Mg(SCN)_2{\cdot}2H_2O{\cdot}2$THF all ligand pairs remain in the *trans* configuration. The magnesium cation, the thiocyanate anion and the THF related oxygen atom are situated on a mirror plane, which leads to a positional disorder of the non-planar THF molecule (Fig. 7b, red and blue atoms and bonds). The complete replacement of water by THF yields a propeller-like complex $[Mg(NCS)_2(THF)_4]$ with magnesium situated on the centre of inversion. Two out of four THF molecules in the *trans* configuration are positionally disordered (Fig. 7c, red and blue atoms and bonds). In all complexes the average bond lengths

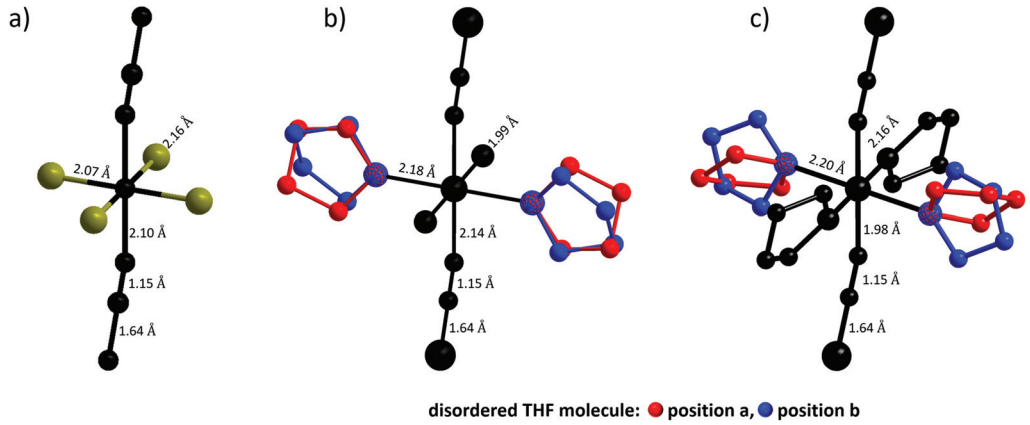

Fig. 7 Octahedral coordination of Mg^{2+} with SCN^-, H_2O and THF in the series $Mg(SCN)_2{\cdot}(4-x)\ H_2O{\cdot}x$THF for (a) $x = 0$, (b) $x = 2$, (c) $x = 4$ (α-phase). Two THF molecules (red and blue atoms and bonds) with identical oxygen positions were used to model the positional disorder.

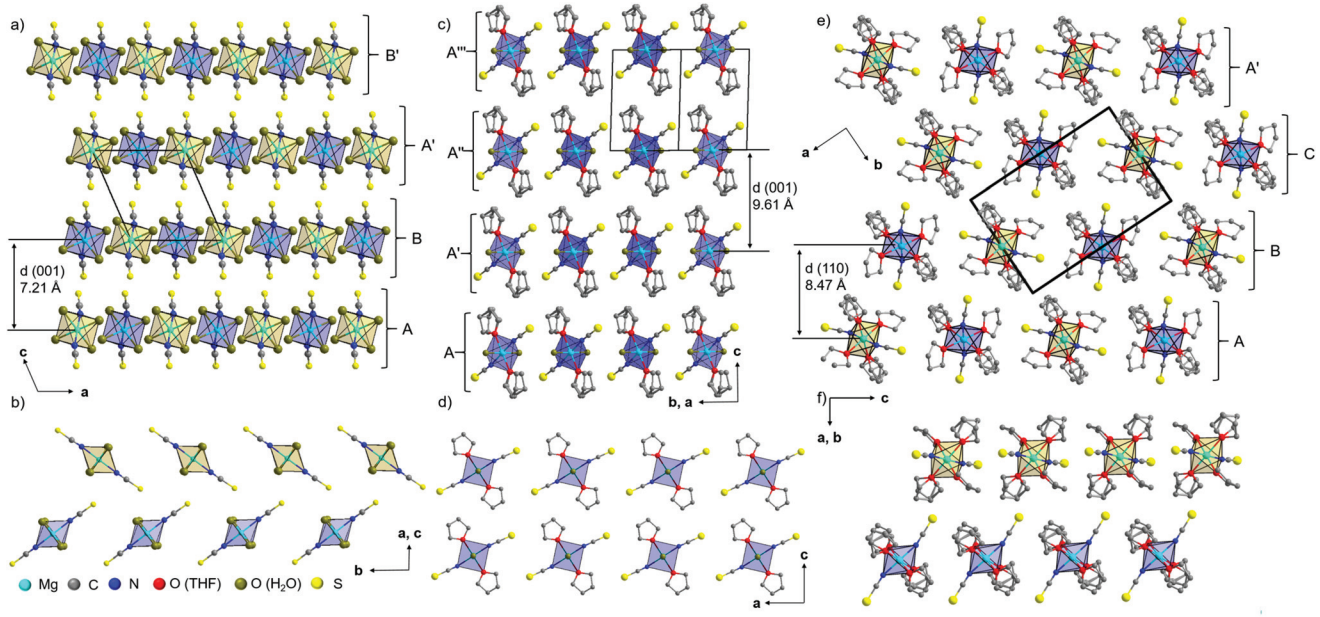

Fig. 8 Packing diagrams in the series $Mg(SCN)_2{\cdot}(4-x)\ H_2O{\cdot}x$THF for (a and b) $x = 0$, (c and d) $x = 2$, (e and f) $x = 4$. Yellow and blue octahedra indicate different orientations, where the thiocyanate ions on top of the blue octahedra point to the front and on the bottom point to the back and the right hand thiocyanates of the yellow octahedra point to the front and the left hand point to the back.

between the central atom and ligands follow this trend: d[Mg–N] < d[Mg–O(H_2O)] < d[Mg–O(THF)], which is to be expected.

In the crystal structures of $Mg(SCN)_2{\cdot}(4-x)\ H_2O{\cdot}x$THF isolated $[Mg(NCS)_2(H_2O)_{4-x}(THF)_x]$ octahedra form layered motifs (Fig. 8). The layers of the tetrahydrate consist of $[Mg(NCS)_2(H_2O)_4]$ octahedra that show an alternating orientation along the *a*-axis (Fig. 8a, blue and yellow octahedra), a uniform orientation along the *b*-axis (Fig. 8b) and are stacked in the [001] direction in a distorted ABA′B′ sequence (ESI, Fig. S11†). The substitution of two water molecules by THF leads to an increase of the inter layer distance. In $Mg(SCN)_2{\cdot}2H_2O{\cdot}2$THF the $[Mg(NCS)_2(H_2O)_2(THF)_2]$ octahedra exhibit a uniform orientation within the layer plane and the layers are stacked in a distorted AA-type fashion (Fig. 8c and d, ESI, Fig. S11†) in the [001] direction. Further replacement of water by THF molecules does not lead to an increase of the inter layer distances. This can be explained by the shift of the AA-stacking order in $Mg(SCN)_2{\cdot}2H_2O{\cdot}2$THF to a distorted ABC-type stacking in $Mg(SCN)_2{\cdot}4$THF (Fig. 8e) in the [110] direction and by an increase of the distances between $[Mg(NCS)_2(THF)_4]$ octahedra within the layers.

In terms of layer constitution and stacking order, $Mg(SCN)_2{\cdot}4$THF (Fig. 8e and f) exhibits strong similarities to $Mg(SCN)_2{\cdot}4H_2O$, whereas $Mg(SCN)_2{\cdot}2H_2O{\cdot}2$THF occupies an exceptional position in the row of $Mg(SCN)_2{\cdot}(4-x)\ H_2O{\cdot}x$THF structures.

Heating of $Mg(SCN)_2{\cdot}4THF$ (α-form) leads to the high temperature modification of β-$Mg(SCN)_2{\cdot}4THF$ and eventually to the formation of $Mg(SCN)_2{\cdot}2THF$ by the release of 2THF molecules. In the crystal structures of the $Mg(SCN)_2{\cdot}x$THF phases, magnesium is always coordinated octahedrally with the thiocyanate anions situated in the *trans* conformation (Fig. 9). The coordination patterns of α- and β-$Mg(SCN)_2{\cdot}4THF$ are almost identical (Fig. 9a and b). In the high temperature phase, all THF molecules are positionally disordered (Fig. 9b, blue and red atoms and bonds). After the release of two THF molecules at higher temperatures, the positional disorder of the remaining THF molecules increases (Fig. 9c, blue, red, yellow and green atoms and bonds), and the thiocyanate anions become positionally disordered as well (Fig. 9c, magenta and violet atoms and bonds). Due to the release of two ligands during the formation of $Mg(SCN)_2{\cdot}2THF$, the emerging voids in the coordination sphere of magnesium are filled by thiocyanate related sulphur atoms, which leads to the formation of thiocyanate bridged $_\infty[Mg(NCS)_{2/2}(SCN)_{2/2}(THF)_2]$ chains (Niggli formula: $^1_\infty\left\{\left[Mg(N,S)^e_{4/2}O^t_{2/1}\right]\right\}$).

The constitution and the packing of the layered motifs are very similar for the room and the high temperature modification of $Mg(SCN)_2{\cdot}4THF$ (Fig. 10a–d) and the seemingly increased interlayer distance after the phase transformation is attributed to the strong thermal expansion of α-$Mg(SCN)_2{\cdot}4THF$ (see below). In the β-form the distorted ABC stack-

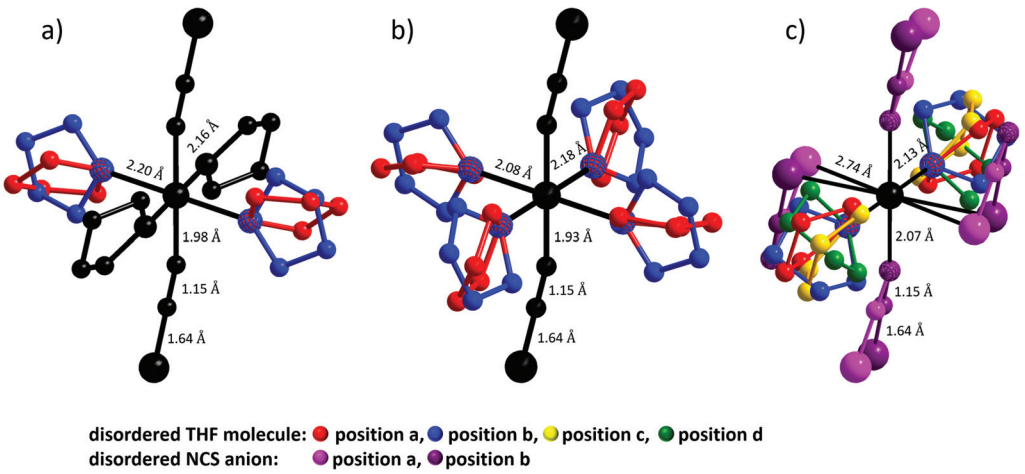

Fig. 9 Octahedral coordination of Mg^{2+} with SCN^- and THF for (a) α-$Mg(SCN)_2{\cdot}4THF$; (b); β-$Mg(SCN)_2{\cdot}4THF$; and (c) $Mg(SCN)_2{\cdot}2THF$. Multiple THF molecules (red, blue, yellow and green atoms and bonds) and of SCN^- anions (magenta and violet atoms and bonds) were used to approximate the positional disorder in the structures.

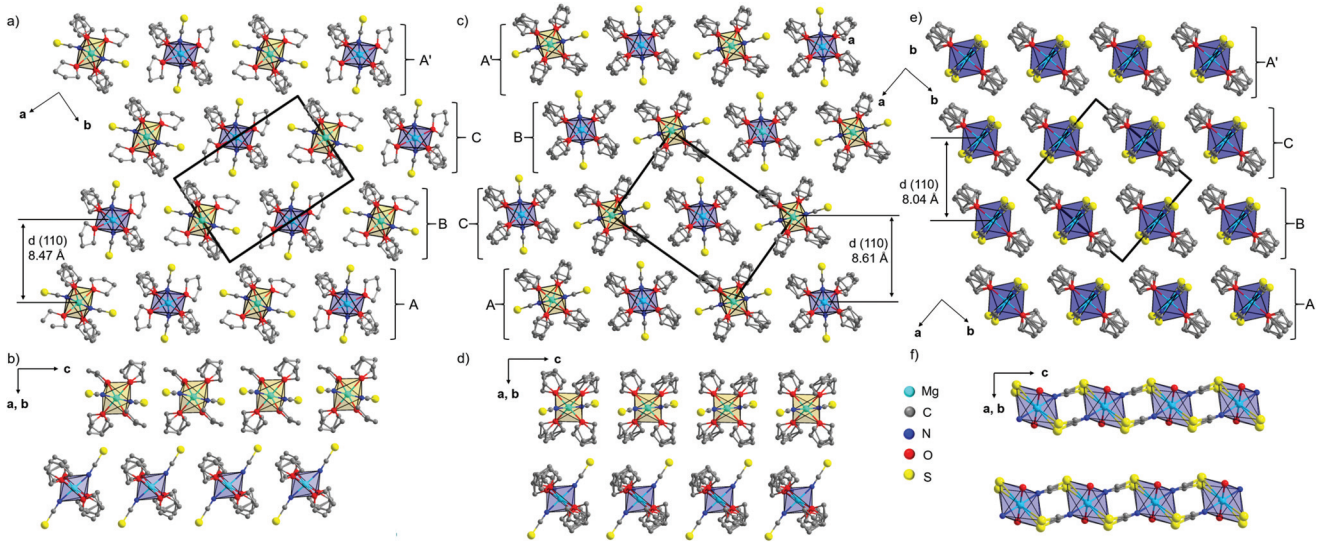

Fig. 10 Packing diagrams of (a and b) α-$Mg(SCN)_2{\cdot}4THF$ at 25 °C, (c and d) β-$Mg(SCN)_2{\cdot}4THF$ at 150 °C and (e and f) $Mg(SCN)_2{\cdot}2THF$ at 180 °C. In (f) the C atoms from the THF molecules are omitted for clarity. Yellow and blue octahedra indicate different orientations, where the thiocyanate ions on top of the blue octahedra point to the front and on the bottom point to the back and the right hand thiocyanates of the yellow octahedra point to the front and the left hand point to the back.

ing sequence of α-$Mg(SCN)_2$·4THF is reverted to a disordered ACB stacking sequence (ESI, Fig. S11†). Releasing two THF molecules from $Mg(SCN)_2$·4THF causes drastic structural changes. In $Mg(SCN)_2$·2THF the $_\infty[Mg(NCS)_{2/2}(SCN)_{2/2}(THF)_2]$ chains are arranged in layers as well with a decreased interlayer distance (Fig. 10e). Within the layers the $[Mg(NCS)_{2/2}(SCN)_{2/2}(THF)_2]$ octahedra are oriented uniformly (Fig. 10e and f). Like β-Mg $(SCN)_2$·4THF, $Mg(SCN)_2$·2THF exhibits a disordered ABC stacking sequence (ESI, Fig. S11†) in the [110] direction.

Lattice expansion

The thermal expansion was investigated in detail for Mg $(SCN)_2$·$4H_2O$, α- and β-$Mg(SCN)_2$·4THF and $Mg(SCN)_2$·2THF. Plots showing the variation of the thermal expansion coefficient (α) with the principal directions X_1, X_2 and X_3 (Table S10†) for these phases are presented in Fig. 11. All compounds exhibit a pronounced anisotropic thermal expansion and some even both positive (Fig. 11, red lines) and negative (Fig. 11, blue lines) thermal expansion. The thermal expansion properties can be correlated with certain aspects of the crystal structures.

$Mg(SCN)_2$·$4H_2O$ exhibits both a large positive thermal expansion of $165(4) \times 10^{-6}$ K^{-1} in the [100] direction, corresponding to the principal X_3 direction and a negative thermal expansion of $-44(2) \times 10^{-6}$ K^{-1} in the [010] direction, corresponding to the principal X_1 direction (Table S10†). Hence, both the positive and negative thermal expansions occur within the layered motifs, whereas the thermal expansion perpendicular to the layers (principal X_2 axes) is only moderate $(32(1) \times 10^{-6}$ $K^{-1})$. Fig. S12† shows four $[Mg(NCS)_2(H_2O)_4]$ octahedra, which are arranged in a diamond motif within the layers. Strong hydrogen bonds between water molecules (dark grey, dashed bonds) and weaker bonds between water molecules and SCN^- related sulphur (light grey dotted bonds) mediate the interactions within the layers. During the thermal expansion the thiocyanate anions start to move slightly out of the layer plains (Table S10,† principal X_2 axes). Accordingly, the $[Mg(NCS)_2(H_2O)_4]$ octahedra, whose thiocyanate anions face in the direction of the centre of gravity of the diamond motif (Fig. S12,† black globe), start to move towards each other (blue arrow, corresponding to the principal X_1 axis). Due to steric reasons and in order to maintain a favourable O–H···S angle close to 180°, the $[Mg(NCS)_2(H_2O)_4]$ octahedra situated along the *a*-axis veer away from the center of gravity (red arrow, corresponding to the principal X_3 axis). With respect to the centre of gravity, the expansion behaviour is comparable to Nuremberg scissors.

A complete exchange of water by THF molecules leads to an increase of the total volume expansion from $153(2) \times 10^{-6}$ K^{-1} to $268(2) \times 10^{-6}$ K^{-1} (Table S10†), which can be explained by the weaker interactions between $[Mg(NCS)_2(THF)_4]$ octahedra. Even though the macroscopic structural motifs α- and β-Mg $(SCN)_2$·4THF are identical (Fig. 10a–d), the thermal expansion properties differ (Fig. 11b and c). Hence the growing disorder of the THF molecules that evolves during the transition from the α- to the β-form has a major impact on the thermal expansion properties. The expansion occurs very anisotropically in α-$Mg(SCN)_2$·4THF (Fig. 11): while there is a strong positive expansion along the principal X_3 axes of $173(1) \times 10^{-6}$ K^{-1} (Table S10†), along the principal X_1 axis, there is hardly any positive thermal expansion $(3(1) \times 10^{-6}$ $K^{-1})$. Within the structure, the strong (Fig. S13a and b,† along X_3 red arrow) and medium (along X_2 green arrow) thermal expansion lead to a beginning shift of the ABC stacking order of the layered motifs towards an ACB stacking. During the phase transition from the α- to the β-form the ordered THF molecule becomes positionally disordered, which leads to a discontinuous increase in the unit cell volume of almost 15 $Å^3$ (Fig. S15†). The ACB stacking order of the β-modification appears to be more favourable with all THF molecules in the structure being disordered. In addition, the complete disorder of the THF molecules leads to a smaller volume expansion of $217(3) \times 10^{-6}$ K^{-1} (Fig. 11c). A strong positive expansion of $128(3) \times 10^{-6}$ K^{-1} occurs along the principal X_3 axis, which corresponds to the [001] direction. Within the layers, rows of equally oriented $[Mg(NCS)_2(THF)_4]$ octahedra (Fig. S13c and d,† red arrows) elongate. The thermal

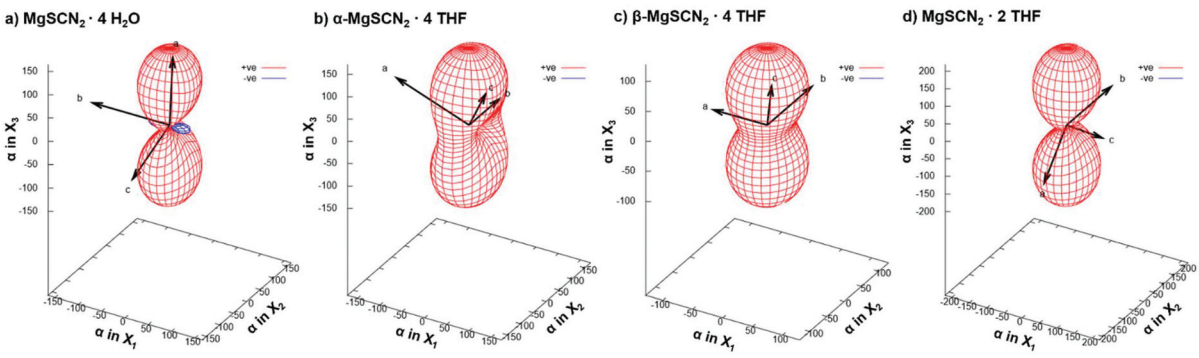

Fig. 11 Plots showing the variation of the thermal expansion coefficient α with the principal directions X_1, X_2 and X_3 (ESI, Table S10 and Fig. S14†) of (a) Mg(SCN)2·$4H_2O$, (b) α-Mg(SCN)2·4THF, (c) β-Mg(SCN)2·4THF and (d) Mg(SCN)2·2THF. Red colour indicates expansion, and blue colour indicates compression.

expansion along the principal X_1 and X_2 axis occurs almost isotropically and corresponds to an expansion both within and in between the layers (Fig. S13c and d,† green arrows).

The release of two THF molecules leads to the formation of one dimensional thiocyanate bridged polyhedra forming $_\infty$[Mg$(NCS)_{2/2}(SCN)_{2/2}(THF)_2$] chains in the crystal structure of Mg$(SCN)_2$·2THF (Fig. 10e and f). This phase shows a negative thermal expansion of $-16(1) \times 10^{-6}$ K^{-1} along these chains (principal X_1 axis) and a strong positive thermal expansion of $219(3) \times 10^{-6}$ K^{-1} perpendicular to the layered motifs (principal X_3 axes, Table S10†). The total volume expansion coefficient of $240(1) \times 10^{-6}$ K^{-1} is larger than in β-Mg$(SCN)_2$·4THF ($217(3) \times 10^{-6}$ K^{-1}) but smaller than in the α-form ($268(2) \times 10^{-6}$ K^{-1}).

Discussion

In the group of alkali and earth alkaline metal thiocyanates, only Be$(SCN)_2$ has not been investigated and magnesium thiocyanate exists exclusively as coordination compounds Mg$(SCN)_2$·x [L]. A close relative is LiSCN, which does exist in its anhydrous form, yet is extremely prone to form hydrates.[18,47] In both cases, the unfavourable bonding between A^{n+} (A = Li, Mg; n = 1, 2) and sulphur atoms in SCN^- is the fundamental reason for their extensive solvent coordination chemistry. The investigations of Mg$(SCN)_2$-coordination compounds reveal a complex thermal decomposition behaviour and disprove any previous claims about the existence of anhydrous Mg$(SCN)_2$.[8–10] To date, Mg$(SCN)_2$·2THF is the only Mg$(SCN)_2$ coordination compound with two solvent ligands, and additionally, the first known Mg^{2+} thiocyanate with Mg–S bonds. Further research of this compound might lead to a procedure to promote Mg–S bonding and successfully isolate anhydrous Mg$(SCN)_2$. The anisotropic thermal expansion properties of the title compounds are interesting as well. Among the thiocyanates, it was already shown that in KSCN the lattice expansion occurs anisotropically with a linear increase until its well-known phase transition.[48] Other studies about the thermal expansion of thiocyanates are rather rare and typically limited to more complex systems, such as multi-cationic or organometallic compounds, which are of interest for nonlinear optics.[49,50] Both in Mg$(SCN)_2$·4H_2O and in Mg$(SCN)_2$·2THF we observed positive and negative thermal expansion, which is not an unusual phenomenon in pseudo halide compounds like $Ag_3[Co(CN)_6]$.[51,52] In addition, there is an order–disorder phase transition in Mg$(SCN)_2$·4THF, which affects the thermal expansion properties. Disorder in coordination compounds is very common, *e.g.* one famous example being the rotational disorder of $[CH_3NH_3]^+$ (MA) in $MAPbI_3$ with its tetragonal to cubic phase transition.[53] The research of ligand disorder and its impact on the parent material's chemistry or properties is very established in extended systems, such as metal–organic frameworks (MOFs),[54] but much rarer in crystalline solids with molecular coordination units. Like other coordination polymers,[55] Mg$(SCN)_2$·2THF exhibits a negative thermal expansion along the chains and a strong positive thermal expansion perpendicular to the chain axis.

In conclusion, the coordination chemistry of Mg$(SCN)_2$ turned out to be rich and has the potential to go beyond H_2O and THF as ligands. Moreover, magnesium is very similar to nickel in terms of ionic radius and preference for an octahedral coordination,[56] so exploring SCN-THF complexes appears to be an excellent opportunity to further expand the rich coordination chemistry of nickel(II) thiocyanates.[57–60] Indeed, similar $M^{II}(SCN)_2$·4THF complexes with M = Ni, V and a $M^{II}(SCN)_2$·2THF phase with M = Co have been found,[61] but the thermal behaviour and the polymorphism have not been investigated yet.

Conclusion

The recrystallization of Mg$(SCN)_2$·4H_2O in THF yields the hitherto unknown compounds Mg$(SCN)_2$·2H_2O·2THF and α-Mg$(SCN)_2$·4THF. While the mixed H_2O-THF phase is very sensitive to heat or moisture, and even slowly decomposes under an Ar atmosphere, the pure THF phase exhibits a higher thermal stability and can be stored under an inert atmosphere for at least several weeks. In the crystal structures isolated Mg$(NCS)_2(H_2O)_{4-x}(THF)_x$ units form layered motifs and magnesium is always situated on the center of inversion or on a mirror plane. The latter might be the reason why Mg$(SCN)_2$·$(4 - x)$ H_2O·xTHF compounds with x = 1 or 3 were not discovered. In the structure of α-Mg$(SCN)_2$·4THF half of the THF molecules are positionally disordered. Heating of the compounds leads to a phase transformation into the β-form between 130 and 135 °C. After the phase transformation, all THF molecules are positionally disordered and the stacking order of the layered motifs is reversed. Further heating eventually leads to the release of two THF molecules at 170 °C. In Mg$(SCN)_2$·2THF thiocyanate related sulfur atoms fill the voids in the coordination sphere of magnesium, which leads to the formation of one dimensional $_\infty$[Mg$(NCS)_{2/2}(SCN)_{2/2}(THF)_2$] chains. Anhydrous Mg$(SCN)_2$ cannot be obtained by further heating as the thiocyanate partially decomposes leading to the formation of a strongly disordered solid that cannot be characterized. All investigated Mg$(SCN)_2$·$(4 - x)$ H_2O·xTHF phases exhibit a remarkable anisotropic thermal expansion, and Mg$(SCN)_2$·4H_2O as well as Mg$(SCN)_2$·2THF were found to show both positive and negative thermal expansion. The order–disorder transition of the THF molecules during the transformation from α- to β-Mg$(SCN)_2$·4THF has a major impact on the thermal expansion properties, *i.e.* it reduces the overall volume expansion and makes it more isotropic.

Author contributions

The manuscript was written through contributions of all authors. All authors have given approval to the final version of the manuscript.

Conflicts of interest

There are no conflicts to declare.

Acknowledgements

We want to thank and acknowledge all contributors for the making of this report: Helga Hoier and Claus Mühle (XRPD), Viola Duppel, Bernhard Fenk and Ulrike Waizman (SEM-EDX), as well as Marie-Luise Schreiber (IR). Thank you all for your useful contributions. Open Access funding provided by the Max Planck Society.

Notes and references

1 P. A. Agron and W. R. Busing, *Acta Crystallogr., Sect. C: Cryst. Struct. Commun.*, 1985, **41**, 8–10.
2 K. Sugimoto, R. E. Dinnebier and J. C. Hanson, *Acta Crystallogr., Sect. B: Struct. Sci.*, 2007, **63**, 235–242.
3 R. K. Motkuri, R. S. Vemuri, D. Barpaga, H. Schaef, J. S. Loring, P. F. Martin, D. B. Lao, S. K. Nune and B. P. McGrail, *ACS Sustainable Chem. Eng.*, 2018, **6**, 1048–1054.
4 M. Pannach, S. Bette and D. Freyer, *J. Chem. Eng. Data*, 2017, **62**, 1384–1396.
5 T. S. Daloee and F. K. Behbahani, *Mol. Divers.*, 2020, **24**, 463–476.
6 A. Unmack, D. M. Murray-Rust and H. Hartley, *Proc. R. Soc. London, Ser. A*, 1930, **127**, 228–240.
7 K. Mereiter and A. Preisinger, *Acta Crystallogr., Sect. B: Struct. Crystallogr. Cryst. Chem.*, 1982, **38**, 1263–1265.
8 D. R. Schultz and R. W. Parry, *J. Am. Chem. Soc.*, 1958, **80**, 4–8.
9 K. Yoshihara, H. Ohshima, N. Momozawa, H. Sakai, K. Nishiyama and M. Abe, *Colloid Polym. Sci.*, 1996, **274**, 685–695.
10 S. C. Mojumdar, M. Melník and E. Jóna, *J. Anal. Appl. Pyrolysis*, 1998, **46**, 147–156.
11 S. C. Mojumdar, M. Melník, E. Jóna and D. Hudecová, *Chem. Pap.*, 1999, **53**, 265–271.
12 D. V. Soldatov, P. A. Trushin, V. A. Logvinenko and E. V. Grachev, *J. Struct. Chem.*, 1993, **34**, 232–238.
13 K. Touaj and M. Chabanel, *J. Chem. Soc., Faraday Trans.*, 1995, **91**, 4395–4401.
14 C. Wickleder and P. Larsen, *Chem. Mater.*, 2004, **16**, 4016–4021.
15 S. Gunasekaran and S. Ponnusamy, *Cryst. Res. Technol.*, 2006, **41**, 130–137.
16 U. Berger and W. Schnick, *J. Alloys Compd.*, 1994, **206**, 179–184.
17 B. Jürgens, E. Irran and W. Schnick, *J. Solid State Chem.*, 2001, **157**, 241–249.
18 O. Reckeweg, A. Schulz, B. Blaschkowski, Th. Schleid and F. J. DiSalvo, *Z. Naturforsch., B: J. Chem. Sci.*, 2014, **69**, 17–24.
19 K. Mereiter and A. Preisinger, *Z. Kristallogr.*, 1984, **169**, 95–107.
20 S. Yamamoto, M. Sakuno and Y. Shinnaka, *J. Phys. Soc. Jpn.*, 1987, **56**, 4393–4399.
21 C. Wickleder and P. Larsen, *Z. Naturforsch., B: J. Chem. Sci.*, 2002, **57**, 1419–1426.
22 C. Wickleder, *Z. Anorg. Allg. Chem.*, 2001, **627**, 1693.
23 E. Dubler, A. Reller and H. R. Oswald, *Z. Kristallogr.*, 1982, **161**, 265–277.
24 I. Lindqvist, *Acta Crystallogr.*, 1957, **10**, 29–32.
25 A. L. Beauchamp and D. Goutier, *Can. J. Chem.*, 1972, **50**, 977–981.
26 K. Sasvári and G. A. Jeffrey, *Acta Crystallogr.*, 1966, **20**, 875–881.
27 H. Schmidt, E. Hennings and W. Voigt, *Acta Crystallogr., Sect. C: Cryst. Struct. Commun.*, 2012, **68**, 4–9.
28 E. Hennings, H. Schmidt and W. Voigt, *Acta Crystallogr., Sect. C: Cryst. Struct. Commun.*, 2013, **69**, 1292–1300.
29 M. G. Aranda, I. Artioli, T. Bier, À.G De la Torre, D. Freyer, R. Kaden, B. Lothenbach, C. Pritzel, B. Raab, S. Stöber, J. Södje, P. Stemmermann, T. Westphal, F. Winnefeld and Q. L. Yu, *Cementitious Materials*, De Gruyter, Berlin, Boston, 2017.
30 T. Rüffer, C. Bruhn and D. Steinborn, *Z. Anorg. Allg. Chem.*, 2001, **627**, 2408–2412.
31 K. Czaja, M. Białek and A. Utrata, *J. Polym. Sci., Part A: Polym. Chem.*, 2004, **42**, 2512–2519.
32 W. OchÈ©dzan-Siodłak and M. Nowakowska, *Eur. Polym. J.*, 2005, **41**, 941–947.
33 S. Pirinen, K. Jayaratne, P. Denifl and T. T. Pakkanen, *J. Mol. Catal. A: Chem.*, 2014, **395**, 434–439.
34 M. Salama, I. Shterenberg, L. J. W. Shimon, K. Keinan-Adamsky, M. Afri, Y. Gofer and D. Aurbach, *J. Phys. Chem. C*, 2017, **121**, 24909–24918.
35 S. Halut-Desportes and C. Bois, *Acta Crystallogr., Sect. B: Struct. Crystallogr. Cryst. Chem.*, 1979, **35**, 2205–2207.
36 P. Sobota, T. Pluzinski and T. Lis, *Z. Anorg. Allg. Chem.*, 1986, **533**, 215–224.
37 P. Sobota, J. Ejfler, T. Płuziński and T. Lis, *Polyhedron*, 1991, **10**, 2457–2461.
38 B. Neumüller, G. Stieglitz and K. Dehnicke, *Z. Naturforsch., B: J. Chem. Sci.*, 1993, **48**, 1151–1154.
39 J. M. Bakker, G. B. Deacon, C. M. Forsyth, P. C. Junk and M. Wiecko, *Eur. J. Inorg. Chem.*, 2010, **6**, 2813–2825.
40 E. Shurdha, S. H. Lapidus, P. W. Stephens, C. E. Moore, A. L. Rheingold and J. S. Miller, *Inorg. Chem.*, 2012, **51**, 9655–9665.
41 IUPAC, *Nomenclature of Inorganic Chemistry*, Butterworths, London, 1970, p. 2.
42 D. R. Lide, Physical Constants of Organic Compounds, in *CRC Handbook of Chemistry and Physics, 90th Edition (CD-ROM Version 2010)*, CRC Press/Taylor and Francis, Boca Raton, FL, 2010.

43 Solubility KCl, https://periodic-table-of-elements.org/SOLUBILITY/potassium_chloride, (accessed 5 September 2020).
44 M. Chaplin, Water Absorption Spectrum, http://www1.lsbu.ac.uk/water/water_vibrational_spectrum.html, (accessed 5 September 2020).
45 A. Palm and E. R. Bissell, *Spectrochim. Acta*, 1960, **16**, 459–466.
46 L. H. Jones, *J. Chem. Phys.*, 1956, **25**, 1069–1072.
47 D. A. Lee, *Inorg. Chem.*, 1964, **3**, 289–290.
48 W. Schranz, in *Phase Transitions*, 1994, vol. 51, pp. 1–66.
49 X. Wang, D. Xu, Y. T. Chow, W. Liu, S. Li, J. Huang, G. Zhang, M. Lü, D. Yuan, H. P. Chan, Q. Ren and P. L. Chu, *Mater. Res. Bull.*, 2004, **39**, 1407–1416.
50 X. Q. Wang, X. F. Cheng, S. J. Zhang, D. Xu, G. H. Zhang, Z. H. Sun, F. P. Yu, X. J. Liu, W. L. Liu and C. L. Chen, *Physica B: Condens. Matter*, 2010, **405**, 1071–1080.
51 A. L. Goodwin, M. Calleja, M. J. Conterio, M. T. Dove, J. S. O. Evans, D. A. Keen, L. Peters and M. G. Tucker, *Science*, 2008, **319**, 794–797.
52 A. L. Goodwin, D. A. Keen and M. G. Tucker, *Proc. Natl. Acad. Sci. U. S. A.*, 2008, **105**, 18708–18713.
53 A. Poglitsch and D. Weber, *J. Chem. Phys.*, 1987, **87**, 6373–6378.
54 R. E. Morris and L. Brammer, *Chem. Soc. Rev.*, 2017, **46**, 5444–5462.
55 K. Yadava, G. Gallo, S. Bette, C. E. Mulijanto, D. P. Karothu, I. H. Park, R. Medishetty, P. Naumov, R. E. Dinnebier and J. J. Vittal, *IUCrJ*, 2020, **7**, 83–89.
56 R. D. Shannon, *Acta Crystallogr., Sect. A: Cryst. Phys., Diffr., Theor. Gen. Crystallogr.*, 1976, **32**, 751–767.
57 C. Wellm, T. Neumann, M. Ceglarska, G. Gallo, M. Rams, R. E. Dinnebier and C. Näther, *CrystEngComm*, 2020, **22**, 2350–2360.
58 C. Wellm and C. Näther, *Acta Crystallogr., Sect. E: Crystallogr. Commun.*, 2019, **75**, 1685–1688.
59 A. Jochim, M. Ceglarska, M. Rams and C. Näther, *Z. Anorg. Allg. Chem.*, 2018, **644**, 1760–1770.
60 A. Jochim, M. Rams, T. Neumann, C. Wellm, H. Reinsch, G. M. Wójtowicz and C. Näther, *Eur. J. Inorg. Chem.*, 2018, **2018**, 4779–4789.
61 E. Shurdha, C. E. Moore, A. L. Rheingold, S. H. Lapidus, P. W. Stephens, A. M. Arif and J. S. Miller, *Inorg. Chem.*, 2013, **52**(18), 10583–10594.